Dispersion engineered slot photonic crystal waveguides for slow light operation

Charles Caer[1], Xavier Le Roux[1], Laurent Vivien[1], Eric Cassan[1]

[1]Institut d'Electronique Fondamentale, Univ. Paris-Sud, CNRS, Bât. 220, F91405 Orsay, France
*corresponding author, E-mail: charles.caer@u-psud.fr

Abstract

We introduce a novel design of wide Slot Photonic Crystal Waveguides (SPCW) by structuring the slot as a comb. This allows performing dispersion engineering in order to achieve very low group velocities over a few nanometers bandwidth. This kind of SPCW offers opportunities to realize devices requiring strong interactions between light and an optically non-linear low index material by providing an ultra-high optical density while easing the filling of the slot due to its width. We will present dispersion engineering results by Plane Wave Expansion method and Finite Difference Time Domain analysis, followed by experimental realization.

1. Introduction

Photonic Crystals Waveguides (PCW) operating in slow light regime are promising devices for all-optical signal processing and enhanced light-matter interactions [1]. However, the issue of propagation losses at low group velocities is still challenging their generalization, whereas it has partially addressed by dispersion engineering [2]. The strong dependence of the nonlinear phase shift on the group velocity gives rise to strong benefits of slow light for nonlinear operations [3]. This gain can be further enhanced with the introduction of a slot, allowing the use of nonlinear polymers with higher figures of merit than silicon [4]. Indeed, for $\chi^{(2)}$ nonlinear polymers, efficient electrooptic modulation has already been successfully reported [5-6].

Opening a slot along the line defect of PCW pulls the fundamental mode of the slot within the photonic bandgap [7]. This slope is positive in the First Brillouin Zone (FBZ), unlike the standard defect mode. Depending on the slot width, these two guided modes with the same even symmetry can coexist [8], but the W1 defect mode exits the photonic bandgap in case of large slots. The latter has received more interest than the slot one, because of the stronger optical confinement in narrow slots and an easier coupling from/to a photonic nanowire. Due to a stronger confinement in narrower slots and an easier coupling, the W1 defect band has received more interest [5-6,8-9]. But wider slots improve the poling efficiency of $\chi^{(2)}$ polymers and are more easily filled [6].

We report here a method to obtain a SPCW with wide slot, i.e. > 150 nm, operating in a flat band slow light regime. We realize this dispersion engineering by adding corrugations to the slot, similar to Bragg gratings. This provides three additional degrees of freedom and allows tailoring the guided mode in order to obtain a flat band group index curve. It is shown that these corrugations improve the localization of the electric field along the waveguide direction.

We engineer the dispersion curves of the two modes, because the W1 defect mode presents an easier coupling from a strip waveguide due its mode profile and this mode is guiding light when the slot is narrow, whereas the "slot" mode is relevant when the slot is very large, which can be required in applications such as sensing despite a lower coupling efficiency, as explained in [10].

2. Dispersion engineering of the slot

2.1. Introduction of a slot mode

The SPCW is optimized through calculations performed by Plane Wave Expansion method using the MPB software [11] for a quasi-TE polarization. Eigenmodes are calculated in the unit cell depicted in fig. 1, consisting in a Silicon On Insulator (SOI) slab with a lower silica layer and an upper cladding layer (e.g. polymer), with indices $n_{Silicon}$=3.48, n_{Silica}=1.44 and $n_{Polymer}$=1.6, respectively. The slab thickness h is fixed to 260 nm, the lattice constant a=400 nm, and the hole radius r is 120 nm to ensure a wide TE bandgap. As explained in our previous work [12], the optimization process begins with the choice of the desired slot width W_{slot}. For technological reasons, it is preferable to work with large slots, at least larger than 150 nm. This requires an enlargement of the line defect in order to keep the guided mode within the photonic bandgap. Therefore, we change the W1 defect to W1.25, i.e. a width of $1.25\sqrt{3}a$.

2.2. Tuning the slot mode

The W1.25 photonic crystal waveguide is taken as a starting point. We then calculate the dispersion diagram for increasing values of W_{slot}, in order to evaluate the suitable W_{slot} value giving a flat dispersion curve under the light line to the "slot" mode. The dispersion curve is progressively flattened for increasing W_{slot} values, as the frequency values increase near the edge of the FBZ at k=0.5. The optimum is found around W_{slot}=0.4a because for larger values, the dispersion curve slope becomes positive. In the same time, the increasing values of W_{slot} reject the W1 defect

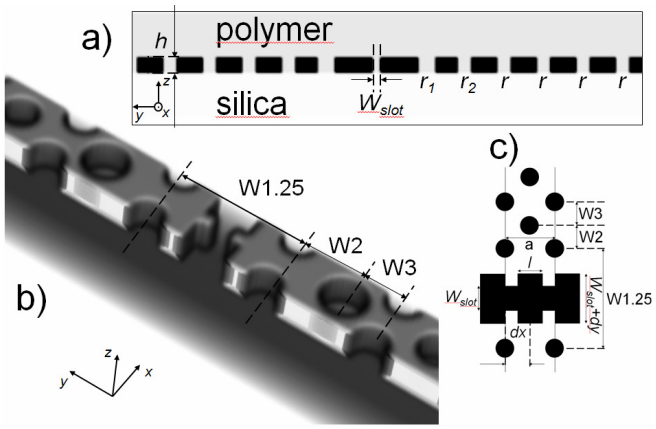

Figure 1: Schematic draw of the unit cell with all relevant parameters in the *yz* plane.

mode outside the photonic bandgap when it reaches W_{slot}=0.4*a*. Next, it is here necessary to pre-compensate the slope of the guided mode before introducing corrugations to the slot by shifting the W2 and W3 hole rows. Forecoming simulations indeed show that decreasing the two values of W2 and W3 (which are nominally equal to $0.5\sqrt{3}a$) makes the slope negative under the light line.

We then introduce corrugations on the slot as described in fig. 1. The comb possesses three parameters: the duty cycle *l*, the depth *dy* of the gratings, and the displacement *dx* of the comb grating regards to the center of the first hole row. It is crucial to keep the periodicity of the comb exactly the same as that of the photonic crystal. Therefore, the bandgap remains controlled by the hole lattice, and the comb provides the three additional degrees of freedom previously mentioned for dispersion engineering. Results about the obtained group index values by considering W1.25, W2=W3=$0.4\sqrt{3}a$, W_{slot}=0.4*a*, dx=0, *l*=0.8, *dy*=0.35*a*, respectively, are reported on fig.2. By referring to the definition of the group index bandwidth product (GBP):

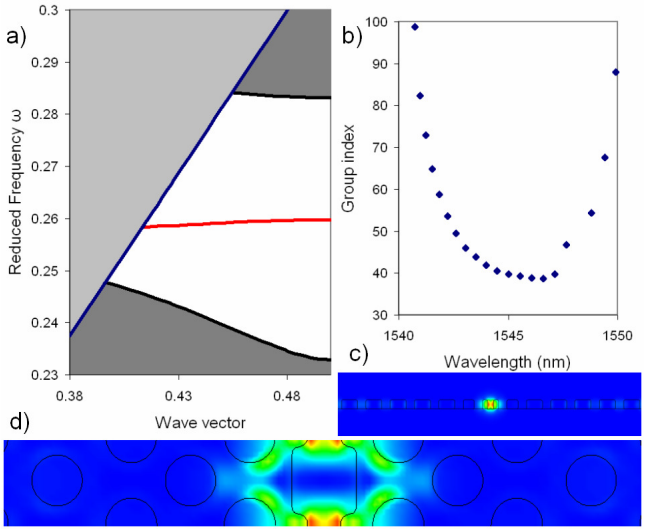

Figure 2: a) Band diagram of the dispersion engineered slot mode. b) Corresponding group index. c) Cross-section of the $\varepsilon|\mathbf{E}|^2$ pattern at *k*=0.45 in the *yz* plane. d) Same pattern viewed in the *xy* plane.

$$GBP = \langle n_g \rangle \frac{\Delta\omega}{\omega_0}, \qquad (1)$$

where $\langle n_g \rangle$ stands for the average group index over a bandwidth $\Delta\omega$ and ω_0 the central wavelength, we obtain a GBP of 0.139. It has to be kept in mind that this GBP is not as large as in some previous studies [2] because of the cladding layer index considered here ($n_{Polymer}$=1.6) which enlarges the light cone compared to air cladding, thus reducing the available bandwidth.

We express the optical confinement [12] by defining the ratio of optical power within the slot over the total power, and the optical intensity *I* as divided by the cross-section of section of the slot, i.e. $h*W_{slot}$ with *h* the height of the silicon slab. We include the effect of electromagnetic density enhancement due to slow light propagation by setting this confinement as the product of the previous optical intensity and the group index n_g for the m-th mode:

$$\eta_m = \frac{n_{g,m}}{hW_s} \frac{\int_{comb} \left(\varepsilon(r)|E_m(r)|^2\right) d^3r}{\int_{cell} \left(\varepsilon(r)|E_m(r)|^2\right) d^3r} \qquad (2)$$

We find here for our structure a confinement factor of 144 μm^{-2}, for an in-slot confinement of 15% of the total power. We recall for comparison that in the case of total internal reflection slot waveguide with the same slot width, the confinement factor is only around 10 μm^{-2}, representing a fifteen-fold enhancement of the confinement. Interestingly, compared to SPCW without any structuration of the slot, the narrowing of the slot provides a stronger confinement of the mode along the waveguide direction, as seen on fig. 2 d). Despite an expectable increase of the scattering losses, it still remains interesting since the modal volume becomes strongly reduced by this structuration, and the same goes for the nonlinear effective area of the guided mode.

2.3. Tuning the W1 mode

Similar dispersion engineering to the one presented in the previous section can be applied to tune the W1 defect mode. The origin of this mode being different, it is less sensitive to the structuration of the comb, when the mode is far from the air band. Nevertheless, we can apply the same procedure. We start with the choice of an adequate slot width, the slope is adjusted by changing the values of W2 and W3, and finally, we tailor the comb. If we want to engineer the dispersion of a SPCW with a wider slot, it is better to work with an enlarged PCW channel, e.g. W1.4, but we lose the benefit of a stronger localization of light at the narrowing, and it is harder to tailor the W1 defect mode which is more sensitive to the modification of the hole array. Moreover, a W1.25 defect still strongly reduces the overlap between the mode and the holes, and leaves the slot as the main source of scattering, then reducing the losses if compared to W1 SPCWs. After structuring the slot, we can see that the parameter *dx* affects the mode profile. An optimum confinement is found when *dx*=0.5*a,* as depicted on fig. 3. This means that where the mode is naturally localized in the slot, adding a corrugation there will strongly enhance the local intensity in the slot, even more if the comb duty cycle

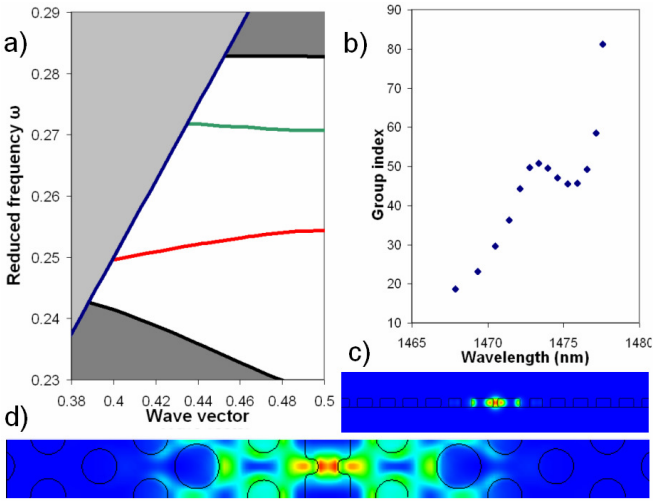

Figure 3: a) Band diagram of the dispersion engineered W1 defect mode (green curve). b) Corresponding group index. c) Cross-section of the $\varepsilon|\mathbf{E}|^2$ pattern at k=0.45 in the yz plane. d) Same pattern viewed in the xy plane.

l is increased, leading to very sharp corrugations. We finally tune the mode to obtain a flat band group index curve by reducing the radius r_1 of the first hole row to 0.28a and by increasing the radius r_2 of the second hole row to 0.38a, similarly to [9]. In this case, with the following parameters: W1.4, W2=0.65, W3=0.45, W_{slot}= 0.35a, dx=0.5a, dy=0.4a, l=0.75, r_1=0.28a, r_2=0.38a, we obtain a mean group index of 48 over a bandwidth of 4.5 nm, giving a GBP of 0.147. This configuration gives a field concentration of 13% in the slot, and a confinement factor of 177 µm^{-2}. We do not exploit the "slot" mode in this case, although present in the photonic bandgap, since the shape of the comb decreases the confinement of the mode in the slot, thus reducing its interest.

3. FDTD Analysis

After optimization of the guided mode in the SPCW, it is a necessity to compute the transmission of a complete device for the evaluation of the propagation losses. The transmission spectrum of the photonic crystal waveguide is calculated by Finite Difference Time Domain simulation using the MEEP software [13]. The implemented structure is shown on fig. 4. It consists of a SPCW with input and output waveguides. The strip waveguides are converted by a 15 µm long taper into slot waveguides with a high coupling efficiency [14] in order to convert adiabatically the mode within the slot, at the input and output of the SPCW. Then, the slot waveguide mode can be coupled to the SPCW one using two transitions regions to adapt the fast light propagation to a slow light regime by slightly stretching the PC lattice in the longitudinal direction [15]. In the injection zone, and next to the reflection zone, the lattice constants a_{inj} and a_{refl} are stretched to 420 nm and 410 nm, respectively, while the lattice constant a remains 400 nm in the central part of the SPCW. As a whole, the length of the photonic crystal crystal waveguide is 88.7µm, which keeps the device footprint to an acceptable value, and the length of the

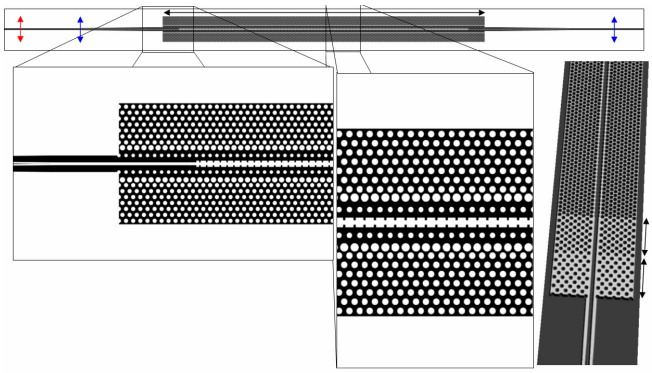

Figure 4: Representation of the FDTD computational cell with different detailed views. The source and the sensors are highlighted in red and blue, respectively.

complete structure with all sub-regions is 177.5 µm. The computational cell is wide enough to avoid coupling with the Perfectly Matched Layers. We perform here 2D FDTD calculations with slab effective index approximation for two reasons: 3D FDTD is excessively time consuming for long devices and out-of-plane losses are not a drawback, since we work exclusively under the light line and backscattering is the main source of losses. The effective index of the silicon in the present case is evaluated to 2.83 by slab optical mode solver. The simulation time range is 70 ps (i.e. 50,000 c/a time units) and the source is a broadband gaussian pulse centered at 1,550 nm with a spectral width of 500 nm. The sensors have a resolution of 50 pm. The grid resolution is 20 nm per pixel. This represents a computation time of 50 hours on 16 CPU. The parameters of the photonic crystal are W1.4, $W2$=0.65, $W3$=0.45, $r1$=0.25a, $r2$=0.38a, r=0.3a, and those of the comb are W_{slot}=0.4a, dy=0.5a, dx=0.5a, and l=0.75. The engineered SPCW has a "W1" mode with group index *plateau* of 45 over 5 nm as shown in fig. 5 and calculated by PWE method. The group index dependence with respect to the bandwidth is extracted from the Fabry-Perot fringes as described in [16]. The transmission is around -12dB, even close to the band edge, confirming the efficiency of the mode conversion and a low level of intrinsic losses and coupling losses. However, we find a mismatch between the group index curves calculated by

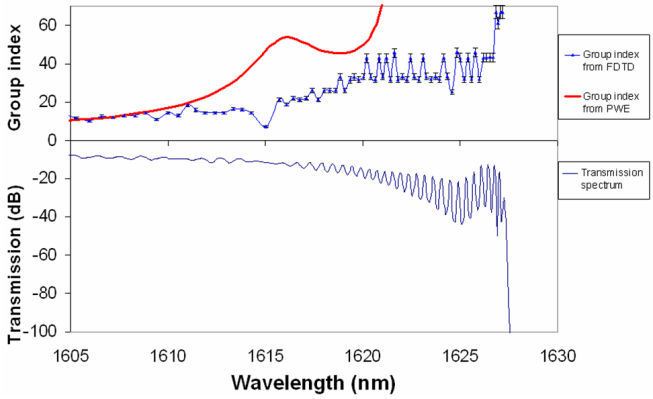

Figure 5: Up: group indices obtained by PWE calculation (red curve) and FDTD calculation (blue dotted curve). Down: corresponding FDTD transmission spectrum.

PWE and FDTD methods due to a difference of the definition of the computation grid, making hard to retieve the same flat band group index curve with the same parameters obtained by PWE. Moreover, the band edge is shifted of approximately 5 nm. However, we retrieve a flat band group index curve by FDTD calculation, confirming the operation in slow light regime with a mean group index of 35 on a 6 nm bandwidth. We underline here that the running time is a critical parameter for the observation of the interference fringes: indeed, physically, the slow pulse needs to reach the output in order to be detected by the sensor. Therefore, group indices above 70 are not consistent. However, this computation gives a good estimation of the level of coupling and intrinsic losses in the SPCW and shows that it is possible to manipulate slow light by FDTD method by directly linking it to the transmission spectrum.

4. Conclusions

We have demonstrated that a comb photonic crystal waveguide is a suitable structure for strongly confining light in a low index material. We have shown that a proper dispersion engineering of the slot itself ensures a flat band group index curve, enabling a slow light operation over a a few nanometers bandwidth. Two structures relying on two different guided modes have been presented. They are operating in slow light regime with group indices of 40 and 48 over bandwidths of 5 nm and 4.5nm, respectively, with slot widths above 140 nm at the narrowest parts. In-slot optical confinements of 15% and 13 % are reported. The slot enlargement is not realized at the expense of a low optical intensity, and the narrowing of the slot into the comb presents a high localization of the electric field, which is of interest for configurations requiring small modal volume and nonlinear effective area.

Finally, FDTD calculations showed an efficient mode conversion from the photonic wire to the SPCW and a high transmission near the band edge. The simulated structure shows slow light operation with a flat band group index of 35 over a bandwidth of 6 nm and a transmission of -12 dB at the band edge. The high localization of the electric field will offer a good opportunity for sensing devices and nonlinear optical effects.

The next task is to work towards the experimental achievement of slow light propagation in a dispersion engineered comb photonic crystal waveguide by analyzing the interference fringes in a Mach-Zehnder Interferometer.

Acknowledgements

Charles Caer acknowledges a scholarship from the French Ministry of Education and Research.

References

[1] T.F. Krauss, Slow light in photonic crystal waveguides, *J. Phys. D: Appl. Phys.* 40: 2666–2670, 2007.

[2] S.A. Schulz, L. O'Faolain, D.M. Beggs, T.P. White, A. Melloni, T.F. Krauss, Dispersion engineered slow light in photonic crystals: a comparison, *J. Opt.* 12: 104004-1-10, 2010.

[3] C. Monat, B. Corcoran, D. Pudo, M. Ebnali-Heidari, C. Grillet, M.D. Pelusi, D.J. Moss, B.J. Eggleton, T.P. White, L. O'Faolain, T.F. Krauss, Slow Light Enhanced Nonlinear Optics in Silicon Photonic Crystal Waveguides, *IEEE J. Sel. Top. Quantum Electron.* 16: 344-356, 2010.

[4] J. Leuthold, W. Freude, J.-M. Brosi, R. Baets, P. Dumon, I. Biaggio, M.L. Scimeca, F. Diederich, B. Frank, C. Koos, Silicon Organic Hybrid Technology - A Platform for Practical Nonlinear Optics, *Proc. of the IEEE*, 97:1304-1316, 2009.

[5] J.-H. Wülbern, S. Prorok, J. Hampe, A. Petrov, M. Eich, J. Luo, A.K.-Y. Jen, M. Jenett, A. Jacob, 40 GHz electro-optic modulation in hybrid silicon–organic slotted photonic crystal waveguides, *Opt. Lett.* 35: 2753-2755, 2010.

[6] X. Wang, C.-Y. Lin, S. Chakravarty, J. Luo, A.K.-Y. Jen, R.T. Chen, Effective in-device r33 of 735 pm/V on electro-optic polymer infiltrated silicon photonic crystal slot waveguides, *Opt. Lett.* 36: 882-884, 2011.

[7] A. Di Falco, L. O'Faolain, T.F. Krauss, Dispersion control and slow light in slotted photonic crystal waveguides, *Appl. Phys. Lett.* 92: 083501-1-3, 2008.

[8] J. Gao, J.F. McMillan, M.-C. Wu, J. Zheng, S. Assefa, C.W. Wong, Demonstration of an air-slot mode-gap confined photonic crystal slab nanocavity with ultrasmall mode volumes, *Appl. Phys Lett.* 96: 051123-1-3, 2010.

[9] J.-M. Brosi, C. Koos, L.C. Andreani, M. Waldow, J. Leuthold, W. Freude, High-speed-low voltage electro-optic modulator with a polymer infiltrated silicon photonic crystal waveguide, *Opt. Express* 16: 4177-4191, 2008.

[10] M. Scullion, A. Di Falco, T. F. Krauss, High Efficiency Interface for Coupling Into Slotted Photonic Crystal Waveguides, *IEEE J. Photon.*3: 203-208, 2011.

[11] S.G. Johnson, J.D. Joannopoulos, Block-iterative frequency-domain methods for Maxwell's equations in a planewave basis, Opt. *Express* 8: 173-190, 2000.

[12] C. Caer, X. Le Roux, V.K. Do, D. Marris-Morini, N. Izard, L. Vivien, D. Gao, E. Cassan, Dispersion Engineering of Wide Slot Photonic Crystal Waveguides by Bragg-like Corrugation of the Slot, *IEEE Photon. Technol. Lett.* 23: 1298-1300, 2011.

[13] A. F. Oskooi, D. Roundy, M. Ibanescu, P. Bermel, J. D. Joannopoulos, S. G. Johnson, A flexible free-software package for electromagnetic simulations by the FDTD method, *Comput. Phys. Commun.* 181: 687-702, 2010.

[14] Z. Wang, N. Zhu, Y. Tang, L. Wosinski, D. Dai, S. He, Ultracompact low-loss coupler between strip and slot waveguides, *Opt. Lett.* 34: 1498-1500, 2009.

[15] J.-P. Hugonin, P. Lalanne, T.P. White, T.F. Krauss, Coupling into slow-mode photonic crystal Waveguides, *Opt. Lett.* 32: 2638-2640, 2007.

[16] Y.A. Vlasov, S.J. McNab, Coupling into the slow light mode in slab-type photonic crystal waveguides, *Opt. Lett.* 31: 50-52, 2006.